

Marc. S. Weinberg¹
Draper Laboratory,
Cambridge, MA
e-mail: mweinberg@draper.com

Conrad Wall
Massachusetts Eye and Ear Infirmary,
Boston, MA
and
Harvard Medical School,
Boston, MA

Jimmy Robertsson
Massachusetts Eye and Ear Infirmary,
Boston, MA

Edward O'Neil
Draper Laboratory,
Cambridge, MA

Kathleen Sienko
Massachusetts Eye and Ear Infirmary,
Boston, MA
and
Massachusetts Institute of Technology,
Cambridge, MA

Robert Fields
Draper Laboratory,
Cambridge, MA

Tilt Determination in MEMS Inertial Vestibular Prosthesis

Background: There is a clear need for a prosthesis that improves postural stability in the balance impaired. Such a device would be used as a temporary aid during recovery from ablative inner-ear surgery, a postural monitor during rehabilitation (for example, hip surgery), and as a permanent prosthesis for those elderly prone to falls. Method of approach: Recently developed, small instruments have enabled wearable prostheses to augment or replace vestibular functions. The current prosthesis communicates by vibrators mounted on the subject's trunk. In this paper we emphasize the unique algorithms that enable tilt indication with modestly performing micromachined gyroscopes and accelerometers. Results: For large angles and multiple axes, gyro drift and unwanted lateral accelerations are successfully rejected. In single-axis tests, the most dramatic results were obtained in standard operating tests where balance-impaired subjects were deprived of vision and proprioceptive inputs. Balance-impaired subjects who fell (into safety restraints) when not aided were able to stand with the prosthesis. Initial multi-axis tests with healthy subjects have shown that sway is reduced in both forward-back and sideward directions. Conclusions: Positive results in initial testing and a sound theoretical basis for the hardware warrant continued development and testing, which is being conducted at three sites. [DOI: 10.1115/1.2378922]

Introduction

Medical. There is a clear need for a prosthesis that improves postural stability in the balance impaired. Basic uses for balance prostheses include (1) a vestibular "pacemaker" to reduce dizziness and imbalance due to abnormal fluctuations in the peripheral vestibular system, (2) permanent replacement of vestibular function, (3) temporary replacement of motion cues that commonly occur following ablative surgery of the inner ear, and (4) vestibular/balance rehabilitation. In terms of postural control, the primary use of a prosthesis would be to prevent falls. Over 90 million Americans will seek medical attention for dizziness, a malfunction of the inner ear, at least once in their lifetime. The development of small micromachined inertial sensors, gyroscopes, and accelerometers enabled the development of vestibular prostheses, which are described herein.

The inner ear's vestibular system provides cues about self-motion that help stabilize vision during movement. These cues also enable us to orient ourselves with respect to our surroundings, which helps us to stand and walk (Fig. 1). Each inner ear can sense in three dimensions, angular motion and the sum of forces due to linear acceleration and gravity [1]. The central nervous system (CNS) can process these motion cues to estimate self-motion in six degrees of freedom (DOF)—three angular and three linear. When the inner ear, the neural pathways that connect the inner ear to the CNS, or the part of the CNS that processes self-motion information malfunctions due to injury, disease, or prolonged exposure to altered gravity, motion cues are lost or dis-

torted. This lack of sensory information can result in dizziness, blurred vision, inability to orient correctly (including the ability to align with the vertical), and reduced ability to stand or walk, especially under difficult conditions.

Some of these outcomes can have serious consequences, such as increasing the risk of falling. Because current treatments are not completely effective, there is a clear need for a prosthesis to help people with balance problems, including those recovering from ablative inner ear surgery, those with no vestibular inputs, and the elderly, who are prone to falls. A recent analysis [2] of the National Health Interview Survey [3] reports that 6.2 million Americans report chronic (3+ months) problems with dizziness or balance. To be conservative, if only 5% of them could benefit from some form of balance prosthesis, more than 300 000 devices would be needed.

A survey of 9198 community-dwelling, working age people chosen randomly from six large general medical practices found that 0.2% had dizziness severe enough to deserve treatment and were willing to submit to testing and rehabilitation [4]. It is reasonable to assume that this same population would at least be willing to consider the use of a balance aid.

Figure 1 depicts a simplified version of the vestibular system. The simplified motion sensor includes an inertial element, a restoring element (represented by the two spring symbols), and the sensory hair cells whose motion is coupled to the inertial element. Motion of the subject in space, represented by the arrow at the top left of the figure, causes a displacement of the inertial element from its rest position (indicated by the two misaligned vertical arrows). This displacement hyperpolarizes or depolarizes the hair cells, which in turn modulate the spike activity of the first-order vestibular afferents. Thus, motion information travels on the 8th nerve via Scarpa's Ganglion (shown by three cell bodies) to the vestibular nucleus (enclosed by dashed lines) in the CNS. The

¹Corresponding author. Draper Laboratory, Mail Stop 37, 555 Technology Square, Cambridge, MA, 02139, 617.258.2308.

Contributed by the Bioengineering Division of ASME for publication in the JOURNAL OF BIOMECHANICAL ENGINEERING. Manuscript received April 1, 2005; final manuscript received May 8, 2006. Review conducted by Philip V. Bayly.

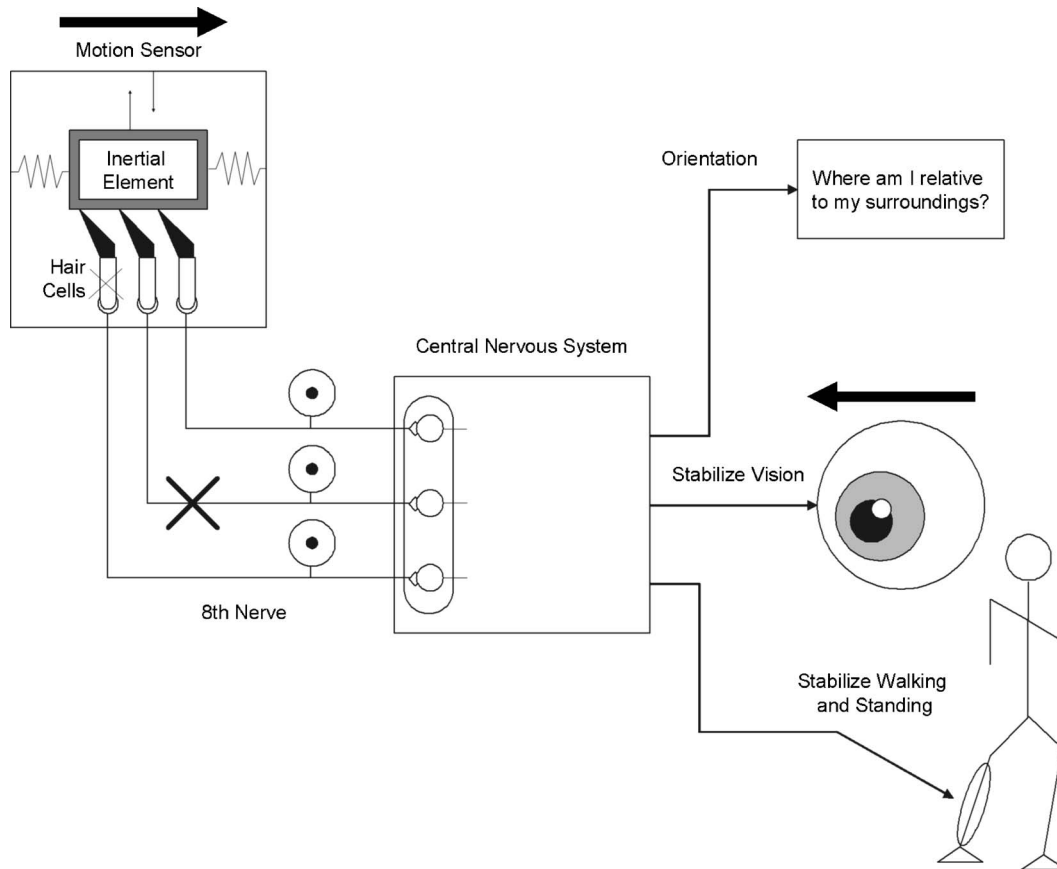


Fig. 1 The vestibular function. Only one of six inertial sensors (otoliths and semicircular canals) on one side is shown. The X indicates a break in the neural path

CNS integrates information necessary for: (1) spatial orientation, (2) stabilization vision (represented by the arrow that points in a direction that is compensatory to the sensed motion), and (3) maintaining postural control. Disease or injury can disrupt the peripheral three-link chain (inertial element, hair cells, and nerve) of motion information, as represented by the X's. A prosthesis would restore lost motion information.

Both implantable and nonimplantable prostheses are currently under consideration. By "implantable prosthesis," we specifically mean a prosthesis that delivers self-motion cues to the CNS via implanted stimulators. This has a number of advantages over reliance on nonvestibular sensory inputs or assisting devices such as canes. These advantages include portability, intuitive operation, replacement of lost natural function, and the ability to work with existing CNS circuitry. Risks of implantable devices include hearing loss due to damage of the hearing transduction process or to the auditory nerve, damage to the vestibular nerve fibers due to mechanical or electrical trauma, and the general risks associated with surgery [5]. One possible side effect is "cross talk," in which the signal that is supposed to stimulate a certain vestibular end organ also stimulates another.

Nonimplantable prostheses are a less invasive means of providing some self-motion cues. They include stimulating the vestibular nerve via surface electrodes or by displaying self-motion cues using "sensory substitution" (e.g., acoustic inputs or electric currents applied to the tongue [6,7]). Stimulation using auditory cues is also being investigated [8]. In the Massachusetts Eye and Ear Infirmary (MEEI) and Draper device, tactile vibrators (tactors) are mounted on the patient's torso and are described further under "The Prosthesis" [9]. Vibrotactile displays have been used suc-

cessfully by the U.S. Navy to furnish navigational cues that allow blindfolded pilots to control their aircraft [10,11], a task with similarities to postural control.

The Prosthesis. The vestibular prosthesis (Figs. 2 and 3) consists of the following elements:

1. The three gyros and three accelerometers instrument sensor assembly (ISA) mounted on the back. Only recently, micro-machining or microelectromechanical systems (MEMS) has enabled these sensors (described in [12]) to become small enough to enable a wearable prosthesis. The instrument sensor assembly includes readout electronics and digitizers and a mechanism and bubble level for aligning the instruments with the patient's natural or comfortable vertical. For the wearable prostheses, two ISAs have been obtained. The low-cost assembly was constructed in-house from Analog Devices ADXL accelerometers and Silicon Sensing Systems gyroscopes. The manufacturer lists accelerometer thermal sensitivity as 3 milligravity (mg) per °C and noise at $0.23 \text{ mg}/\sqrt{\text{Hz}}$. The angular rate sensor is specified as $650 \text{ deg/h}/^\circ\text{C}$ and noise at $470 \text{ deg/h}/\sqrt{\text{Hz}}$. These performance figures are typical for sensors used in automobiles for airbag deployment and traction control. The total volume was $8 \times 10^{-5} \text{ m}^3$ (5 in.³). For a better performance, 8 cubic inch ($1.3 \times 10^{-4} \text{ m}^3$) HG1920 ISAs [13,14] were purchased from Honeywell. Based on Draper MEMS technology, the HG 1920 incorporates accelerometers whose thermal sensitivity is $0.3 \text{ mg}/^\circ\text{C}$ and gyroscopes whose thermal sensitivity and noise are $10 \text{ deg/h}/^\circ\text{C}$ and $5^\circ/\text{h}/\sqrt{\text{Hz}}$, performance

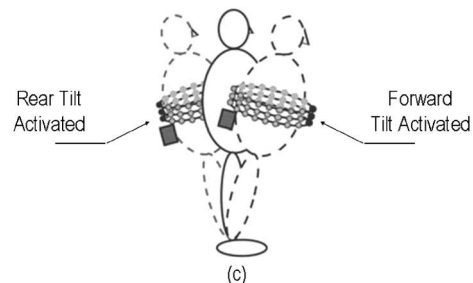
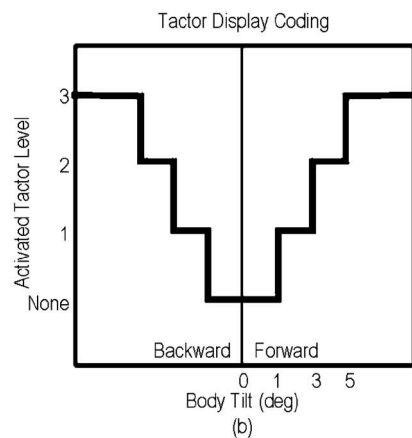
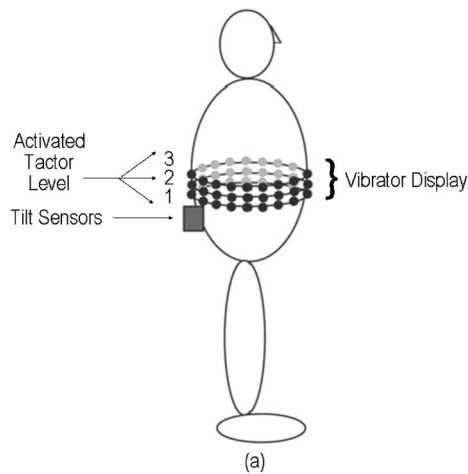


Fig. 2 Tactor coding: (a) tactor locations, (b) the schedule of tilt activation versus tilt magnitude, (c) an example where forward and backward activate only the forward-most and backward-most columns of tactors

one to two orders of magnitude better than commercial automotive-grade sensors. Honeywell and Draper are working to improve sensor performance while reducing the volume to 2 in.³ (3.3×10^{-5} m³) [15].

Preliminary calculations and limited experience indicated that the lower cost instruments should be suitable for a balance prosthesis; however, the higher performance instruments were obtained if better performance were needed. Since the instruments' costs are decreasing rapidly, we did not want to discard the prosthesis concept based on costs that would decrease in coming years.

2. Mechanical vibrators known as tactors or tactaids, which are Food and Drug Administration (FDA)—approved for use in a sensory substitution hearing aid. The tactors are mounted in a belt about the subject's waist.

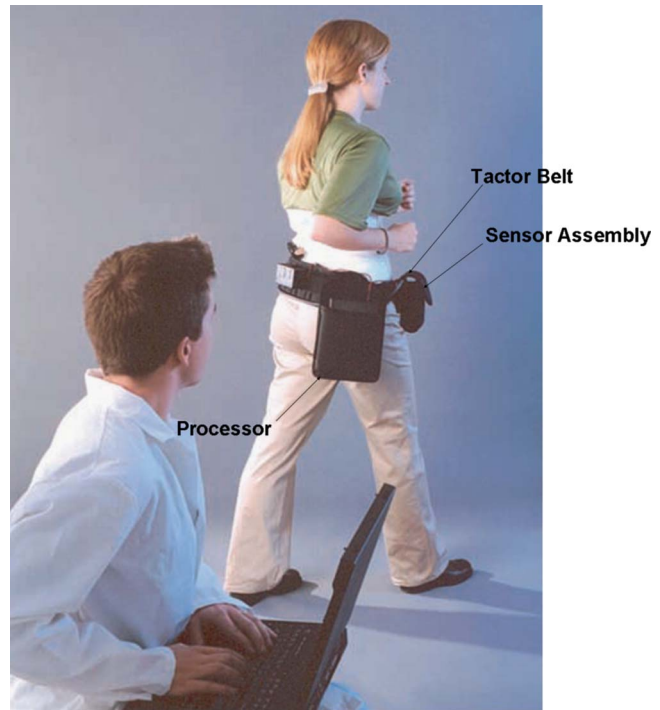


Fig. 3 Major components of the wearable device to show mounting locations. Also shown is the laboratory computer that communicates wirelessly with the wearable device

3. A controller area network (CAN) bus and controllers to send information between the sensors, the central processor, and the tactors.
4. An on-board processor, which executes unique algorithms to detect vertical while rejecting errors caused by instrument drift and extraneous acceleration.
5. Wireless transmission, which allows system parameters such as dead zone and control loop gains to be adjusted and that allows the subject's performance to be recorded remotely.
6. Batteries that supply power to the sensors, processor, and tactors.

For the current prototype system, the locations of sensors and tactors are shown in Fig. 2. The wearable prosthesis is photographed in Fig. 3. At the day's start, the patient is held stationary for one second to align the sensors with the patient's comfortable vertical. The gyro and accelerometer signals are processed to obtain a tilt-angle estimate accurate to within 2 mrad over a 0 to 10 Hz bandwidth. Unique algorithms have been coded to detect tilt with respect to gravity and angular rotation. The wearable prosthesis contains inertial sensors and algorithms that allow large angle operation over long times. The algorithms greatly reduce the impact of gyro bias errors (which could integrate to large angular errors) and lateral accelerations (which could introduce incorrect phase to the control loops). These unique algorithms are this paper's focus. The digital controller commands individual tactor amplifiers, which drive tactors mounted in columns on the subject's front and back at 250 Hz, a sensitive frequency for human skin [16,17]. The tilt's direction is transmitted to the patient by azimuth and the magnitude by the vertical tactors. As a research tool, the number of tactors is operator selectable.

Algorithms For Finding Vertical. The vestibular prosthesis' objective is to sense the vertical and to furnish tilt time derivatives that can be used for damping ("Inverted Pendulum Model" below). Herein, tilt is defined as rotations about horizontal axes. Estimating tilt with only inertial instruments has been described [18–22] for robotics and human subjects. Determining tilt is simi-

lar to but different from the attitude determination for vehicles [23–30] or limb orientation [31,32]. Algorithms for measuring moments and torques are distinct from those used to determine orientation [33].

It has long been recognized that gyroscopes provide excellent angular data at high frequencies, while accelerometers indicate tilt well at low frequencies where extraneous accelerations are not present. For sensing tilt, gyroscope-only solutions have not been satisfactory because the instrument output is angular rate. Because angular rate must be integrated to obtain angle, a calibration error or a shift in the instrument bias (the output with no angular rate input) results in large angular errors rather quickly. Because of lateral acceleration, accelerometer-only solutions do not yield a wide bandwidth tilt indication. The following techniques for combining accelerometers and gyroscopes have been used.

1. *Inertial guidance:* For navigation over periods longer than a few hours, gyros and accelerometers can be combined to realize a vertical indicator that is insensitive to linear acceleration, also known as the space integrator and Shuler pendulum in the classic navigation solution [34,35]. To indicate vertical to 0.001 rad requires very good gyroscopes (better than 0.01 deg/h stability over the 84-min Schuler period). These instrument specifications are out of scope for MEMS devices.
2. *Attitude references:* Attitude reference requires azimuth (angular orientation about the vertical) in addition to two tilts. Because accelerometers cannot detect the angle about the vertical, azimuth information is obtained by adding three magnetometers or Global Positioning System (GPS) radio navigation to the inertial sensors assembly. The angular information obtained from the accelerometers and magnetometers or GPS (generally low frequency) is used to increment the angular information calculated from the gyros. This data fusion is generally done by Kalman filters [28,29] or by least squares fitting [23], which minimizes the differences between the gyrodetermined angles and those determined by the other sensors. Attitude references that are composed of only magnetometers and accelerometers [27,31] work poorly when acceleration, in addition to gravity, is present.
3. *Tilt systems:* For many applications, such as the balance prosthesis, azimuth is not required; however, poor knowledge of azimuth rate generally corrupts tilt estimation. This corruption is caused by the transformation of the gyro rates to tilt angles once the ISA is rotated from its null position. Techniques that look for quiet portions of the accelerometer data to update the gyroangles or quaternions have been employed [19,20,32]. Luinge [18] employed a Kalman filter that was too simple to greatly reduce the effect of gyro drift.

Using modestly performing gyroscopes and accelerometers, an efficient, robust algorithm for estimating tilt over large angles when azimuth is not required is this paper's unique contribution. References [21,36,37] start with assumptions similar to ours about the frequency separation of gravity and accelerations and about rotations (quaternions) defined about horizontal and vertical axes; however, the realization of these assumptions differs from those described in "Methods."

Prosthesis Development. The prototype development has proceeded in several stages. The use of vibrotactile feedback for postural control was chosen because the U.S. Navy successfully applied it to pilot orientation, a task that is somewhat similar to postural control. The first-stage development provided a 1-axis (2-DOF) tilt estimate from a subject-worn rate gyro and accelerometer to a one-axis vibrotactile display mounted on either the front or back of the subject or on the subject's right and left sides. A bench-mounted Powerbook computer was used to process the motion sensor inputs into a tilt estimate and to provide signals that gated an amplifier array that could drive each tactile vibrator with

a 250-Hz signal. This device was used first on control subjects having normal vestibular function, and then on subjects having well-defined vestibulopathies (like a vestibular nerve section or neurectomy). The primary experiments were a single-axis postural control task such as standing heel-to-toe on a narrow rail or taking a standard clinical laboratory balance test, called Computerized Dynamic Posturography Sensory Organization Testing.

The next stage was to modify the benchtop device by adding more degrees of freedom motion sensors and the ability to display two tilt axes to the user (Fig. 2). A typical configuration is a 6-DOF motion sensor package and a spatial resolution for the vibrotactile display of 22.5 deg. This display uses 16 columns of tactors to display tilt direction and 3 levels in each column to display tilt magnitude. The rationale and justification for using three rows of tactors to display tilt magnitude was developed through a separate set of experiments [38]. This device has been used to help determine the spatial resolution of tilt display needed for postural control and for some limited locomotion experiments (by mounting the laptop on a wheeled laboratory cart). From a medical standpoint, all subjects had well-defined vestibulopathies, but were otherwise healthy.

The third stage of device development was to make a completely wearable, battery-powered research prototype device consisting of six body-mounted motion sensors, a PC 104 computer with peripherals, and a 3×16 array of tactile vibrators with amplifiers to drive them (Fig. 3). The primary use of this device is in walking experiments with subjects having well documented vestibulopathies.

In summary, there have been three stages of device development and experiments that involve either control subjects or vestibulopathic subjects that are otherwise healthy. Prior results are discussed in "Results and Discussion, Overview." No efforts have yet been made toward FDA approval (the tactors are already in use on an FDA-approved device) since these devices are still in the research stage.

Technical Options. The technical options fall into two categories: the body tilt to estimate and the method used to display this variable to the user. We estimate the deviation of the body away from the vertical as measured near the subject's center of mass. The rationale is based on the argument that the postural control system aims to keep one's center of mass within one's limits of stability. We actually display the weighted sum of the deviation angle and its first derivative. The rationale for this comes from modeling postural control as a single inverted pendulum (Fig. 4). The single inverted pendulum cannot be stabilized with a restorative torque that is only proportional to the displacement error or just the error rate, but can be stabilized by a combination of proportional plus derivative control.

Possible display options include biofeedback using sound, an array of electrodes mounted on the tongue, a moving visual surround, and an array of tactile vibrators. Our rationale for choosing the latter is that it has been used successfully in aircraft pilot orientation tasks. Vision and hearing displays may divert other useful sensory information from the user, and a tongue device can interfere with talking, drinking, and eating.

Unique Contributions. Several generations of the MEEI/Draper prosthesis have been tested and have reduced sway in vestibulopathic subjects [39–43]. Initial, single-axis tests were done with the patient receiving only information about forward (or sideward) motion. While quantitative results on several standard operating tests have been performed, the most noteworthy result was the ability of vestibulopathic subjects deprived of visual and proprioceptive inputs to stand without falling.

The multiaxis prosthesis was described briefly in [44]. This paper's unique contributions include the following:

1. A unique algorithm for detecting the vertical using only inertial sensors.

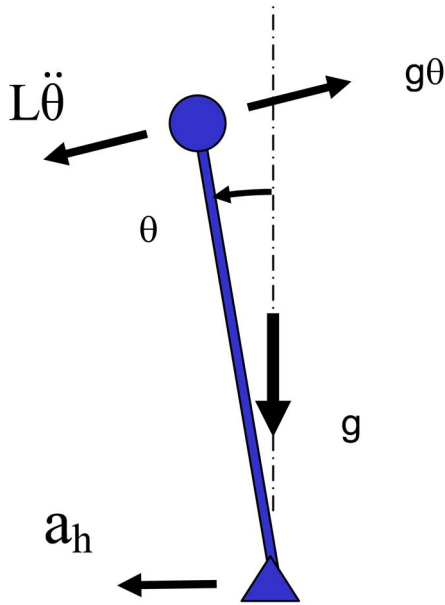


Fig. 4 Inverted pendulum model of standing person

2. Determination of the filter parameters.
3. Application of the algorithm to a multi-axis vestibular prosthesis.

Methods

The prosthesis was described in the Introduction. The instruments and algorithms are selected with the following starting observations:

1. The objective is to find the vertical. Because of the gyroscopes, tilt rate signals will be available. Estimates of yaw are not needed.
2. Gyro-only solutions will not work. With an unknown bias of 100–1000 deg/h typical of MEMS rate sensors, error builds quickly.
3. Accelerometer-only solutions cannot yield a wide bandwidth. At higher frequencies, other accelerations are larger than the tilt effect; for example, subjects are often modeled as an inverted pendulum (Fig. 4). The linear acceleration from angular acceleration is out of phase with tilt and greater than tilt for oscillation greater than 0.4 Hz, as described in Eq. (3).
4. The instrument assembly must be aligned with patient's vertical.

The algorithm will be presented in two steps: single-axis tilt followed by the multi-axis case.

Single-Axis Estimation. A single-axis balance experiment includes an accelerometer whose input axis is nominally orthogonal to gravity and a gyro whose input axis is also horizontal and perpendicular to the accelerometer input axis. The objective is to combine the two outputs to obtain a wide bandwidth estimate of θ , the angle between the patient's vertical and the sensor package. The voltage read from the accelerometer is modeled as:

$$V_a = S_a a + B_a \quad (1)$$

where S_a and B_a are the scale factor and bias of the accelerometer. Assuming small-angle approximations, the input acceleration is given by:

$$a = g(\theta + \alpha) - L\ddot{\theta} + a_h \quad (2)$$

where g =gravity constant (9.8 m/s²),

α =initial offset between accelerometer input axis and patient's vertical,

L =1 to 2 m, which assumes that the subject is modeled as an inverted pendulum, as shown in Fig. 4.

a_h =horizontal acceleration of the pendulum pivot.

The gyro output is modeled as:

$$V_g = S_g \dot{\theta} + B_g \quad (3)$$

where S_g and B_g are the scale factor and bias of the gyro. To obtain a good estimate of tilt θ and to remove the $\ddot{\theta}$ and a_h terms, the acceleration output should be low-pass filtered. For $L=1.5$ m, a typical person, the angular acceleration term in Eq. (2) becomes larger than $g\theta$ for frequencies greater than 0.4 Hz. The $L\ddot{\theta}$ term is 180 deg out of phase with the desired tilt term. For this reason, which is verified by test experience, the break frequency of the low-pass filter is set at 0.03 Hz.

Since the gyro output is integrated, small bias can lead to large angle errors; however, the gyro gives a good estimate of high-frequency rotation. To achieve a wide bandwidth estimate of the tilt angle θ , the gyro and accelerometer signals are combined. In analog Laplace transforms, the tilt is estimated by:

$$\hat{\theta} = \text{LP}(s) \left(\frac{V_a - \hat{B}_a}{\hat{g}\hat{S}_a} \right) + \frac{\text{HP}(s)}{s} \left(\frac{V_g - \hat{B}_g}{\hat{S}_g} \right) \quad (4)$$

where an over caret (^)=estimated or calibrated quantities stored in computation and LP(s) and HP(s) are the transfer functions of the low-pass and high-pass filters.

$$\text{LP}(s) = \frac{s\omega_N^2(2s+1) + \omega_N^3}{(s + \omega_N)(s^2 + 2\zeta\omega_N s + \omega_N^2)} \quad (5)$$

$$\frac{\text{HP}(s)}{s} = \frac{s^2 + s\omega_N(2s+1)}{(s + \omega_N)(s^2 + 2\zeta\omega_N s + \omega_N^2)} \quad (6)$$

The low-pass and high-pass filters are complementary, that is, HP(s)+LP(s)=1. For the single-axis tests, the block diagram of the processing scheme used for the prototype device is shown in Fig. 5. For instructional ease, analog filters are shown. The filters [Eqs. (5) and (6)] are implemented digitally so that the match is accurate. Implementing the gyrofiling as Eq. (6) avoids numerical problems associated with integrating the gyrorate and high-pass filtering later.

For error analysis and calibration, the estimated tilt is obtained from the actual tilt and other poorly modeled effects by substituting Eq. (1) through Eq. (3) into Eq. (4).

$$\hat{\theta} = \text{LP}(s) \left\{ \frac{S_a [g(\theta + \alpha) - L\ddot{\theta} + a_h] + B_a - \hat{B}_a}{\hat{g}\hat{S}_a} \right\} + \frac{\text{HP}(s)}{s} \left(\frac{S_g s \theta + B_g - \hat{B}_g}{\hat{S}_g} \right) \quad (7)$$

Errors in calibration or changes in bias are included in Eq. (7) by including both the actual bias and the bias obtained from calibration. Because of the third-order high-pass filter, Eq. (6), gyro bias errors do not cause a steady shift in the estimated tilt. White gyro noise does not cause angle random walk. The effects of accelerometer noise (the unmodeled bias terms) and angular and lateral accelerations decrease two decades per decade beyond the filter break frequency of 0.03 Hz. For a step input in tilt angle, the

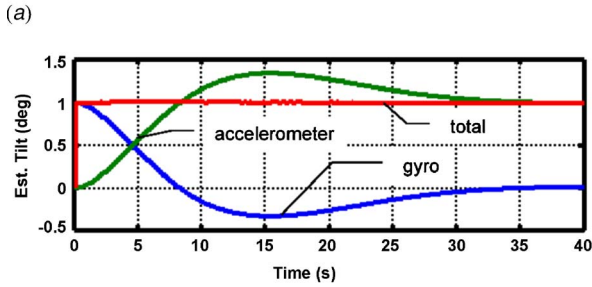
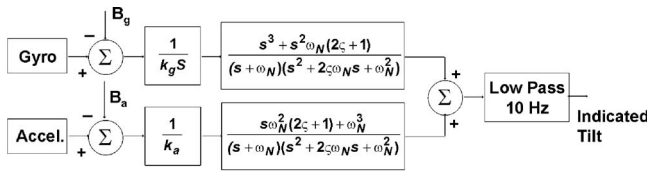


Fig. 5 Single-axis tilt estimation: (a) block diagram (b) the estimated tilts for a 1-deg step change in actual tilt are shown for the gyro, accelerometer, and combined (indicated) channels (simulation)

estimated tilt angles from the gyro and accelerometer channels are plotted in Fig. 5. Undamped natural frequencies of 0.03 Hz, a damping ratio ζ of 0.707, and no bias or scale-factor errors were assumed.

When starting the prosthesis, the patient is held for 1 s at his comfortable vertical; that is, $\theta=0$. Because the patient is still, one assumes that the measured accelerometer voltage equals the accelerometer-estimated bias per Eq. (1). Per Eq. (2), the estimated bias will contain the accelerometer-to-patient misalignment.

$$\hat{B}_a = B_a + S_{ag}\alpha \quad (8)$$

Inserting Eq. (8) into Eq. (7), the calibration has accounted for the misalignment, a result that requires that the accelerometer input axis be close to, but not exactly, horizontal. (If the nominal accelerometer bias is known beforehand, unknown residual alignment is calibrated.) During calibration, a new gyro bias is also determined by Eq. (3). Calibrating the accelerometer and gyro bias greatly reduces any filter [Eq. (7)] startup transients.

The balance prosthesis should estimate the vertical within 0.1 to 1 deg [43]. A 1 mg (0.0098 m/s^2) accelerometer bias shift causes a 0.001 rad (0.06 deg) tilt error. Since the bias is calibrated at instrument turn-on, it must be maintained for roughly 16 h. With 0.03 Hz filtering, accelerometer white noise of $1 \text{ mg}/\sqrt{\text{Hz}}$ results in 0.2 mrad of tilt. One-mg stability represents the best MEMS sensors, while 5 to 50 mg is typical of automotive-grade sensors. Because the gyro signal is filtered to eliminate bias, accelerometer bias, not gyro bias, is the limiting factor in our processing scheme. The gyro contributes only transient errors. With the 0.03 Hz filters, 360 deg/h/ $\sqrt{\text{Hz}}$ gyro white noise, typical of automotive sensors, results in 0.1 deg tilt error. The maximum allowable transient tilt error for a balance-impaired subject to fall are not known.

Multi-Axis Tilt Estimation. For the general multiaxis, large-angle situation, the algorithms were expanded to account for the instrument axes changing their spatial orientation as the patient leans or tilts. From the discussion on single-axis tilt, the accelerometers can remove gyro drift from horizontal gyros. Gravity measurements cannot remove drift from vertical (azimuth sensing) gyros; however, the prosthesis is not interested in azimuth, an observation that can be used to advantage. Incremental tilt (sensed by the gyros) requires knowledge of the tilt magnitudes; that is, the correction sent to the patient requires knowledge of where the

gyroinput axes are.

As an alternative to Euler angles (virtual gimbals) and transformation matrices, quaternions were employed to calculate the rotations. From the gyro or accelerometer outputs, one can directly calculate the quaternions (see Appendix A for details). By separating the orientation into a rotation about the vertical and a rotation about the horizontal, the horizontal quaternion is calculated without knowledge of azimuth and is independent of azimuth gyro drift. As in the single-axis situation, drift in the nominally horizontal gyro is removed by using the accelerometers for low frequencies.

Reference Frames. Define the body frame, indicated by the letter b , as attached to the patient's trunk (or head). When the roll and pitch angles are zero, the x and y body axes are aligned with the roll (forward) and pitch (right) directions and the z axis points down. Vectors in the body frame are transformed into the ISA frame or platform frame through the orthogonal transformation C_b^p [Eq. (13)].

The platform axes (p) define the location of the ISA and are defined by the x and y accelerometer input axes per Eq. (14). The remaining accelerometer axes are not aligned with the platform axes. This small angle transformation from platform to accelerometer axes is defined by the nonorthogonal matrix C_p^a [Eq. (14)]. Similarly, the transformation from the platform to gyro input axes is defined by the nonorthogonal matrix C_p^g [Eq. (15)].

The local coordinate frame is fixed to the earth with the z axis aligned with gravity. For this analysis and physical dimension space, it is valid to consider the earth locally flat.

Gyro Quaternions. A foundation of the actual algorithm will be determined. To separate out the yaw angle, write the quaternion Q_g , which transforms a vector in the platform frame to the local frame by a rotation about the horizontal followed by a rotation about the vertical.

$$Q_g = Q_v * * Q_H \quad (9)$$

where Q_v =rotation quaternion about the vertical

$$= [\cos(\theta/2) \ 0 \ 0 \ \sin(\theta/2)]$$

θ =rotation about the vertical of inertial space with respect to the platform

Q_H =rotation quaternion about the horizontal

$$= [h_1, h_2, h_3, 0]$$

**=indicates quaternion multiplication

The quaternion conventions are listed in Appendix A. Define the angular rate of

$$\vec{\omega}^b = [0, \omega_x^b, \omega_y^b, \omega_z^b] \quad (10)$$

The body rate is measured by the gyroscopes after compensating for bias, scale factor, and angular misalignments. The rotation quaternions are related to the platform rate through (Appendix A):

$$\dot{Q}_g = \frac{Q_g * * \vec{\omega}^b}{2} \quad (11)$$

Substitute Eqs. (9) and (10) into Eq. (11) and solve for the individual quaternion terms.

$$\dot{h}_1 = -\frac{1}{2}(\omega_x h_2 + \omega_y h_3)$$

$$\dot{h}_2 = \omega_z h_3 + \frac{\omega_y h_2 h_3}{2h_1} + \frac{\omega_x}{2} \left(h_1 - \frac{h_3^2}{h_1} \right)$$

$$\dot{h}_3 = -\omega_z h_2 + \frac{\omega_y}{2} \left(h_1 - \frac{h_2^2}{h_1} \right) + \frac{\omega_x h_2 h_3}{2h_1}$$

$$\dot{\theta} = \omega_z + \frac{\omega_y h_2}{h_1} - \frac{\omega_x h_3}{h_1} \quad (12)$$

In Eq. (12), the superscript b has been dropped from the rates in body coordinates. Equation (12) demonstrates the following desirable qualities:

1. None of the time derivatives includes the azimuth angle θ . This will enable the high- and low-pass filtering of gyro and accelerometer signals so that h_1 , h_2 , and h_3 will approach the accelerometer-determined values.
2. The equations do not require algebraic solutions so that integration is straightforward.
3. For estimating tilt, the θ' equation is not required.
4. The h terms transform a vector from the platform coordinates to a frame rotating about the vertical at the yaw rate.

There is a singularity when $h_1=0$, when the platform is rotated ± 180 deg about any horizontal axis; that is, the platform is completely turned over and the subject is standing on his head. When the platform is completely turned over, it cannot determine about which horizontal axis to rotate to right itself. This singularity arises because the quaternion has been split into rotations about the vertical and about the horizontal per Eq. (9). Roll, pitch, and yaw axes enable the separation of azimuth from tilt; however, pitch contains a singularity at ± 90 deg so that Euler angles are not considered further.

Instrument Platform and Sensor Axes. The equations coded to determine tilt in the multiaxis prosthesis are listed. The transformation matrix relating coordinates in the body frame to those of the inertial platform are given by:

$$C_b^p = \begin{bmatrix} 1 & \beta_z & -\beta_y \\ -\beta_z & 1 & \beta_x \\ \beta_y & -\beta_x & 1 \end{bmatrix} \quad (13)$$

where β =rotation about subscripted axis. Small misalignment angles are assumed.

The platform is defined by the direction of the nominally x accelerometer and the direction of the y -axis accelerometer as defined by its rotation about the x axis. The misalignment of the accelerometer input axes with respect to the platform axes are defined by the nonorthogonal matrix:

$$C_p^a = \begin{bmatrix} 1 & 0 & 0 \\ -\alpha_{5z} & 1 & 0 \\ \alpha_{6y} & -\alpha_{6x} & 1 \end{bmatrix} \quad (14)$$

where α =misalignment angle. The number indicates the instrument while the letter indicates the angle about which the input axis is rotated. Subscripts 4–6 denote accelerometers, while 1–3 indicate gyroscopes.

Again, small misalignment angles are assumed. The zero terms in Eq. (14) reflect the definition of the inertial platform and reflect the x and y axes being in the horizontal plane when the ISA platform and body frame are aligned. Including α_{4y} , α_{4z} , and α_{5x} can replace C_b^p and defines the ISA accelerometer axes with respect to another frame such as the table axes.

The misalignment of the gyroscope input axes with respect to the platform axes are defined by the nonorthogonal matrix:

$$C_p^g = \begin{bmatrix} 1 & \alpha_{1z} & -\alpha_{1y} \\ -\alpha_{2z} & 1 & \alpha_{2x} \\ \alpha_{3y} & -\alpha_{3x} & 1 \end{bmatrix} \quad (15)$$

The Sensor Outputs. The outputs of the gyros are obtained by transforming rates from platform to gyro coordinates. Each gyro is modeled as a simple bias plus scale factor. Linear cross-axis terms

are included in the misalignment angles [Eq. (15)]. The platform rates are solved directly from the three instrument voltages.

$$\begin{bmatrix} V_1 \\ V_2 \\ V_3 \end{bmatrix} = \begin{bmatrix} B_1 \\ B_2 \\ B_3 \end{bmatrix} + \begin{bmatrix} S_1 & 0 & 0 \\ 0 & S_2 & 0 \\ 0 & 0 & S_3 \end{bmatrix} C_p^g \begin{bmatrix} \omega_x \\ \omega_y \\ \omega_z \end{bmatrix} \quad (16)$$

where V =instrument output voltage subscripts 1–3 refer to gyros.

B =instrument bias

S =instrument scale factor

ω =rates measured in platform coordinates

Because the accelerometers are low-pass filtered, lateral accelerations and distance from rotation centers are not included. Considering only gravity inputs, the accelerometer outputs are determined by:

$$\begin{bmatrix} V_4 \\ V_5 \\ V_6 \end{bmatrix} = \begin{bmatrix} B_4 \\ B_5 \\ B_6 \end{bmatrix} + \begin{bmatrix} S_4 & 0 & 0 \\ 0 & S_5 & 0 \\ 0 & 0 & S_6 \end{bmatrix} C_p^a \begin{bmatrix} -g_x \\ -g_y \\ -g_z \end{bmatrix} \quad (17)$$

Equation (17) assumes that a plus gravity appears as a negative acceleration. From the accelerometer output voltages, one solves for the three components of acceleration in the platform frame. From the platform gravity vector, define the measured gravity quaternion as:

$$\hat{g}^p = [0 \ \hat{g}_x \ \hat{g}_y \ \hat{g}_z] \quad (18)$$

The quaternion about a horizontal axis for rotating gravity from platform coordinates to earth fixed coordinates is:

$$Q_a = \begin{bmatrix} \cos\left(\frac{\varphi}{2}\right) & \left| \frac{\sin\left(\frac{\varphi}{2}\right)g_y}{\sqrt{g_x^2 + g_y^2}} \right| & \left| \frac{-\sin\left(\frac{\varphi}{2}\right)g_x}{\sqrt{g_x^2 + g_y^2}} \right| & 0 \end{bmatrix} \quad (19)$$

where φ =rotation magnitude

$$\tan(\varphi) = \sqrt{g_x^2 + g_y^2} / g_z, \quad 0 \leq \varphi \leq \pi$$

The zero in the fourth position of Q_a specifies that the rotation is about a horizontal axis. Transforming Eq. (18) by Eq. (19) per Eq. (29) results in $[0 \ 0 \ 0 \ \sqrt{g_x^2 + g_y^2 + g_z^2}]$, a check on the quaternion rotation. The code includes logic to include tracking φ for rotations over the top ($h_1=0$).

Blending of the Quaternions—The Complementary Filter.

The gyro Q_H [Eq. (9)] and accelerometer-derived rotation [Eq. (19)] quaternions are identical in form. Similar to Eq. (4), the total quaternion can be obtained by high-pass filtering the gyro-derived quaternion to remove gyro drift and low-pass filtering the accelerometer-derived quaternion to reduce translation effects.

$$Q_T(s) = L_p(s)Q_a(s) + \frac{H_p(s)}{s} \dot{Q}_g(s) \quad (20)$$

An efficient mechanization of Eq. (20) is presented in Appendix B. The filter break frequency ω_N was set at 0.19 rad/s and the damping ratio ζ at 0.707 Hz for all examples and tests.

The Gyro Quaternion Differential Equations. If poor estimates of quaternions h are used in Eq. (12), the gyro derivative h' will be calculated inaccurately; therefore, the gyro derivatives are obtained from the total quaternions, that is, the gyro quaternion updates [Eq. (12)] are made more specific as:

$$\dot{h}_{1g} = -\frac{1}{2}(\omega_x h_{2T} + \omega_y h_{3T})$$

$$\dot{h}_{2g} = \omega_z h_{3T} + \frac{\omega_y h_{2T} h_{3T}}{2h_{1T}} + \frac{\omega_x}{2} \left(h_{1T} - \frac{h_{3T}^2}{h_{1T}} \right)$$

$$\dot{h}_{3g} = -\omega_z h_{2T} + \frac{\omega_x}{2} \left(h_{1T} - \frac{h_{2T}^2}{h_{1T}} \right) + \frac{\omega_x h_{2T} h_{3T}}{2h_{1T}} \quad (21)$$

where subscript g =gyrobased quaternion

T =total (gyro plus accelerometer-based) quaternion as defined in Eq. (20)

ω_i =angular rates measured by the gyros and transformed into platform coordinates.

Because the accelerometer quaternion [Eq. (19)] is determined from acceleration ratios, its magnitude is always unity, as expected for a rotation quaternion. The total quaternion is normalized to unity, but the gyro quaternion is not. The complementary filter [Eq. (20)] correctly extracts the gyro quaternions' oscillating portion so that the total quaternion is close to one. The gyro quaternions [Eq. (21)] are inserted into the complementary filters [Eqs. (5), (6), and (20)], which are numerically integrated by a second order Runge-Kutta [45].

Firing Factors. The total quaternion is used to determine a total indicated gravity to fire the factors. The gravity in inertial coordinates $[0, 0, 0, g]$ is rotated by the conjugate of Q_T to obtain the gravity in the platform frame. Normalized to unity, the gravity in platform coordinates is calculated from the total quaternion by:

$$\begin{aligned} g_x &= -2h_{1T}h_{3T} \\ g_y &= 2h_{1T}h_{2T} \\ g_z &= h_{1T}^2 - h_{2T}^2 - h_{3T}^2 \end{aligned} \quad (22)$$

The term h_{1T} defines the magnitude of the rotation as described in Appendix A or, by inspection of Eq. (22), all three terms can be employed.

$$\varphi = \text{atan2}(\sqrt{g_x^2 + g_y^2}, g_z) \quad 0 \leq \varphi \leq \pi \quad (23)$$

The firing angle is the azimuth θ , indicating the direction toward which the patient should move. The firing angle is measured from the forward (one or roll) axis about the positive (nominally down) yaw axis and is determined by:

$$\theta = \text{atan2}[g_y, g_x] + \pi = \text{atan2}[-g_y, -g_x] = \text{atan2}[-h_{2T}, h_{3T}] \quad (24)$$

If the roll axis is up while the pitch axis is horizontal, the subject is leaning backward. The acceleration sensed by the x-axis accelerometer is positive, which means the sensed g_x is negative. Agreeing with Eq. (24), the front tactor will be commanded to vibrate. Another example: assume the patient leans forward and right (into the first quadrant). Both x and y accelerometers will indicate positive gravity (negative acceleration). The tactors in the third quadrant will vibrate.

Initialization. The single-axis description of Eqs. (7) and (8) is expanded. The tactors drive the patient to the nulls defined by the sensors' output signals. Because of the complementary filters [Eq. (20)], the low-frequency null (below 0.03 Hz) is determined by the accelerometers. The prosthesis must be initialized to align the patient's comfortable vertical with that indicated by the accelerometers. In addition, the sensors' bias (the output signal when no acceleration or angular rate is applied) can drift between factory (test station) calibration and field tests with patients. Changing instrument bias is equivalent to the instrument's null changing with time.

Beforehand on the test station, the sensors' bias, scale factor, and the misalignment angles with respect to the ISA reference plane are calibrated. Because the tilt algorithms seek to null the sensor outputs, sensor, particularly accelerometer, bias is generally more important than scale factor. In summary, initialization focuses on alignment angles and sensor bias. For the two-axis

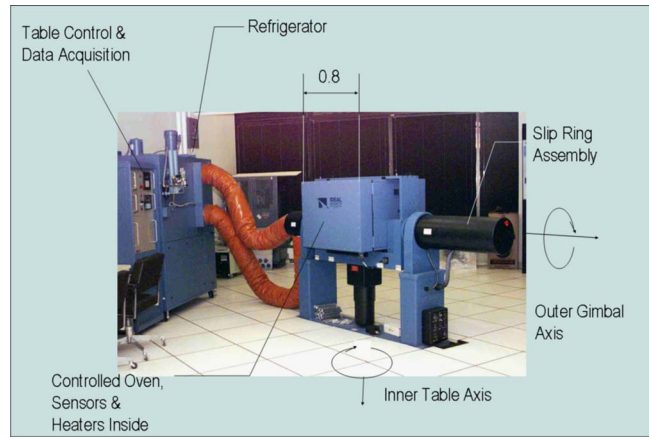


Fig. 6 Two-axis, motion sensor test station equipped for thermal sensitivity testing. The horizontal cylinders drive outer gimbal rotation axis. The vertical cylinder below the station rotates inner table axis. The system under test is inside the cubic, electrically heated thermal enclosure mounted on the inner axis. Seen behind the test station and connected by insulated flexible tubes is the cooler, which enables operation to below -40°C

situation, the stationary calibration can be performed in two ways. One can measure a lumped bias or one can assume the factory bias and determine the body to platform misalignments.

Consider combining the accelerometer bias and alignment angles, which is our usual approach. The ISA is mounted on the patient and is adjusted to be nearly level, as indicated by the bubble level. The leveling implies that the sensor input axes are close to horizontal and vertical; thus, misalignments between the patient's vertical and the ISA are small angles. With assistance, the patient stands vertical for 1 s to accomplish the initialization. With the assumption of no motion, the gyro outputs are recorded as gyro bias. Again, assuming no motion, the horizontal accelerometer outputs contain sensor bias plus misalignment times gravity terms and are automatically entered into the algorithm as a bias (the "lumped" bias). The lumped bias [Eq. (8)] effectively nulls the accelerometers to the patient's comfortable vertical and removes accelerometer drift. At this point, the angles between the accelerometers and patient vertical are not known; however, for low frequency and steady state, the ISA will drive the patient to his vertical. Because the angles are not known, knowledge of the vertical at high frequencies (gyro alignment is assumed small) and high roll and pitch angles is not perfect, but sufficient for null-seeking prostheses. The periodic bias calibration allows less costly instruments to be used.

A second option is to assume that accelerometer bias is constant and does not require periodic recalibration or to provide a simple calibration fixture so that the sensors' bias can be measured immediately before mounting the ISA to the subject. Determining accelerometer bias from input axis up and down is relatively insensitive to alignment angles and can be done without a precise test table. During the on-patient initialization, one can solve for the misalignments of the accelerometers and employ the factory-supplied misalignments of the gyros with respect to the accelerometers. One cannot determine misalignment about the vertical, which is really the azimuth alignment between the tactors and the ISA. Since the tactors are used in closed-loop control, precise knowledge of azimuth alignment is not necessary.

Simulation of Vertical Indication. Results obtained from the vertical indicating filter with simulated data emphasize pertinent characteristics. Bias, scale factor, and misalignments are calibrated on a precision multi-axis inertial instrument test table, such as that depicted in Fig. 6; thus, the largest expected error driver is

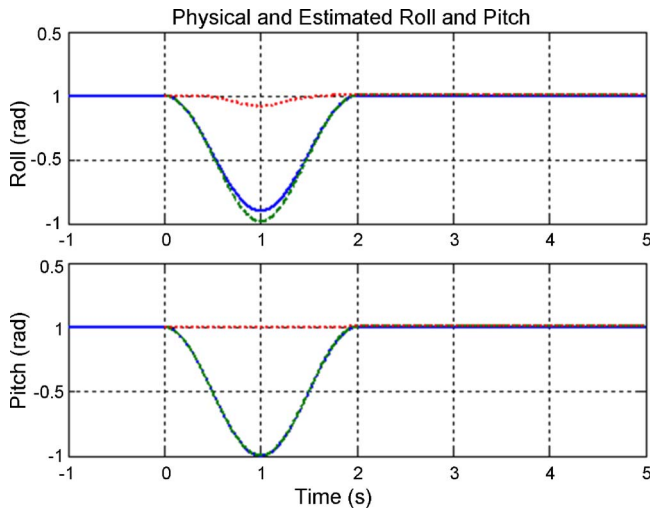


Fig. 7 ISA misaligned 0.1 rad about x , roll (peak -0.9 rad) and pitch (peak -1 rad) motion. Solid line is actual, dashed is estimated, and dotted is difference

the alignment of the instrument sensor assembly to the subject's comfortable vertical. Because test table movement is determined by gimbal angles, the discussion focuses on roll and pitch, although azimuth and elevation are directed to the subject ("Firing Tactor").

In Fig. 7, a 0.1 rad misalignment about the nominal roll axis is assumed. This large misalignment is assumed to emphasize results. Roll and pitch motions whose peaks are -0.9 and -1.0 rad, respectively, excite the ISA. The input and estimated roll and pitch are shown in Fig. 7. The ISA is calibrated for 1 s, so that misalignment is lumped into the accelerometer bias, and no initial attitude error occurs. The peak difference is 0.08 rad; however, the error is zero when the subject returns to null. For smaller motions or misalignments, the peak difference decreases as a fraction of the peak magnitude. For small roll misalignment and no yaw rate, no erroneous rates are coupled into the gyros. For larger angles, the small-angle approximations weaken and errors appear.

In Fig. 8, a misalignment of 0.1 rad about the nominal roll axis is assumed again. About the vertical, the subject rotates at a constant rate of 1 rev/s (turn to the right) for 2 s. For 2 s, the accelerometer contributes little to determining tilt. Because of the misalignment about roll, the vertical rate couples into the pitch gyro. The dynamics propagating the gyro quaternion [Eq. (21)] couple the input rates into both h_{2g} and h_{3g} . The roll and pitch errors are bounded and are approximately equal to the misalignment magnitudes. Because the accelerometer and gyro quaternions lose synchronization, 0.03 rad transients decay with the time constant of the complementary filter.

Finally, consider the response of an ISA with no angular misalignments. Gyro noise is white, 1000 deg/h over a 50 Hz bandwidth (0.01 s sampling), and accelerometer noise is white, 0.01 g over 50 Hz. Because a calibration is performed for 1 s prior to taking data, the fixed biases drop out; however, because of the wide bandwidth noise, the accelerometer and gyro bias are not calibrated perfectly. The calibrated biases are -0.88 and 1.0 mg for the roll and pitch accelerometers, respectively, as seen in the roll and pitch of Fig. 9. Statistically, with a 0.03 Hz low-pass filter, 1 mg rms is expected for the bias. Most of the uncertainty about the mean is attributed to the gyros. Because of the 0.03 Hz filter, the accelerometer noise is calculated as 0.25 mg rms, which is smaller than the data of Fig. 9.

Algorithm Verification on Test Station. The six-instrument tilt algorithm was verified by testing the high-performance HG1920 ISA on a two-axis station (Fig. 6). Although the algorithm con-

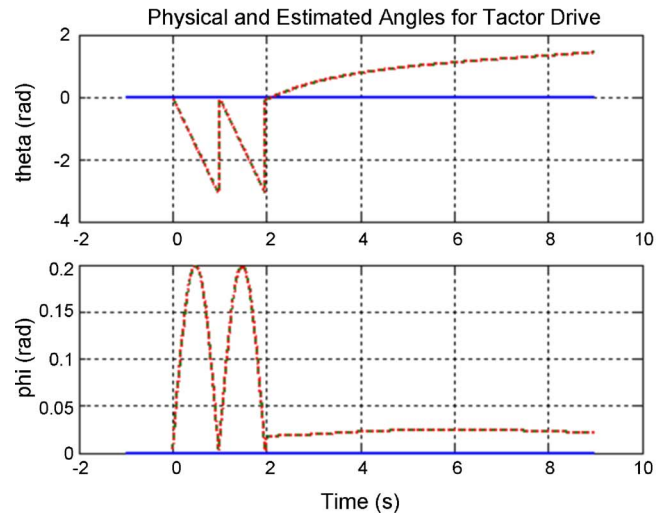
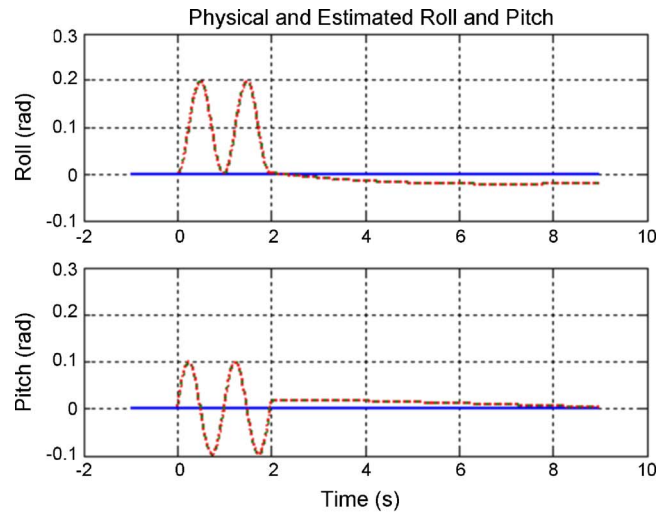


Fig. 8 ISA misaligned 0.1 rad about x , 1 rev/s rotation (turn to right) about vertical. Solid line is actual, dashed is estimated, and dotted is difference

verts quaternions to azimuth and elevation for subjects, the quaternions were converted to table rotation angle for test table to estimated comparison. Figure 10 displays the algorithm output and the table angle for continuous operation during which the table is stepped over angles from 5 to 90 deg. Agreement is excellent. The rapid response at the nearly step inputs is evident and no drift over time has occurred. While errors during the rapid transients are a few degrees because of the 10 Hz frequency rolloff, the step magnitudes are well duplicated to better than 0.2 deg. The test station has been very important in calibrating and verifying the performance of the individual sensors and of the tilt indicating algorithms.

Results and Discussion

Overview. We have previously reported [9,43,44] that the use of vibrotactile tilt feedback (VTTF) can significantly reduce the amount of body tilt in both vestibulopathic and normal subjects when performance is compared with similar test conditions in which VTTF is not provided [9,43,44]. All our previous studies were constrained to display body motion along a single axis (pitch or roll). Several prosthesis generations have been tested and have reduced sway in vestibulopathic subjects [40–44]. The most dramatic finding was that subjects who regularly fell (into safety restraints) during the Sensory Organization Test [46–49] without

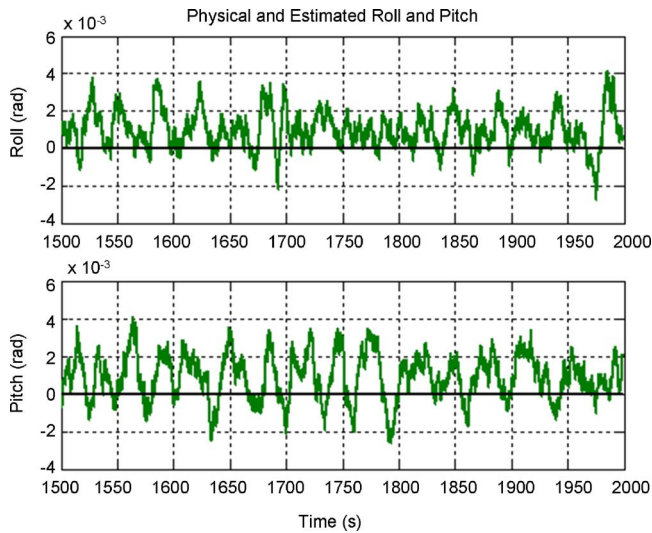


Fig. 9 No misalignments, no inputs. Gyro noise is white, 1000 deg/h over 50 Hz bandwidth (0.01 s sampling), and accelerometer noise is white, 0.01 g over 50 Hz

the aid were able to stand without falling when it was turned on. This is shown in Fig. 11, where falls correspond to a TPI score of zero [43,50]. Preliminary results indicate residual benefits after the prosthesis is removed from balance-impaired patients; that is, the prosthesis has some similarities to training wheels on a bicycle.

The single-axis stationary results have warranted continuation to multiple degrees of freedom with large tilt angles and walking. The objective of this preliminary study was to assess the ability of healthy subjects to control their body tilt under conditions where both the motion of the moving support surface on which they stood and the vibrotactile tactile display of their body motion was in two dimensions instead of one. We had three initial questions: (1) Will use of VTTF result in the reduction of body sway compared with no VTTF during multidirectional surface perturbations? (2) Does the spatial resolution of the VTTF display affect the postural response of the subject given that perturbation and body motion can occur anywhere in a plane? (3) Is there a differ-

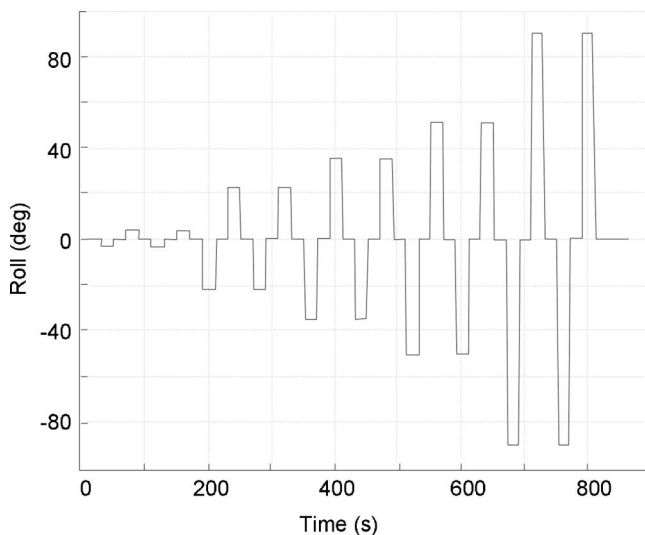


Fig. 10 Test results of higher performance six-axis system for various roll angles. Input and estimated angles are plotted and are very close to one another

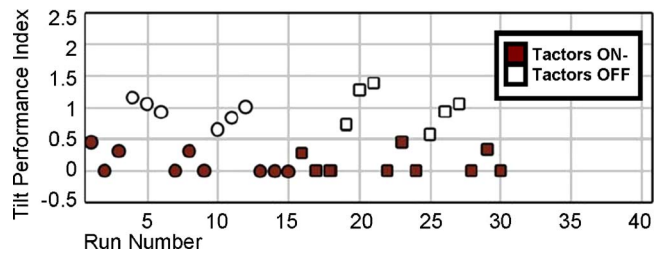


Fig. 11 Sequential tilt performance index (TPI) scores from one subject's sensory organization test (SOT) runs during computerized dynamic posturography testing. The SOT 5 (circles) has distorted proprioceptive and no vision inputs. The SOT 6 (squares) has distorted proprioceptive and visual inputs. $TIP = 1/\text{rms}$ center of pressure sway and is scored zero if the subject falls during a run.

ence in postural performance when VTTF is displayed compared with control trials of repeated exposure to random motion without VTTF?

Human Factors and Training. Successful commercial development of factors to aid those with hearing deficits provided the initial indication that factors could be acceptable for a nonaversive balance aid. Because the factor display rings the torso, it can be concealed easily, which enhances its acceptance. Most users find the vibrotactile display to be very intuitive and learn to use it quickly. Formalized training is done by adapting a commercially available balance rehabilitation device known as the Balance Master. This device dynamically displays an estimate of the subject's center of pressure on a screen. The task of the subject is to "move" the center of pressure around to "hit" a number of preset "targets" on the screen. Our modification of this training has the subject don the vibrotactile vest and experience the combination of visual plus vibrotactile displays while they cycle through the Balance Master targeting tasks. Once subjects master this, the visual display is turned off and the subjects complete the task using just the vibrotactile display. This training procedure typically takes 10 to 20 min, including a familiarization period that precedes the formal task.

Test Description. Two young healthy subjects (1 male, 1 female) with no known vestibular problems and normal scores on Computerized Dynamic Posturography Sensory Organization Tests 5 and 6 were used in a pilot study to assess the efficacy of the MEMS Inertial Vestibular Prosthesis. The Analog Devices accelerometers and Silicon Sensing angular rate sensors were used. Data were collected in the Injury Analysis and Prevention Laboratory in the NeuroMuscular Research Center at Boston University. A custom-built moveable BALANCE DisturbER (BALDER) platform [51] delivered a 30 s low-pass filtered white noise signal generated by the MATLAB® *rand* function and sampled at 100 Hz.

Tilt estimates were displayed on the subjects' torsos via a 3 row \times 16-column factor array (Figs. 2 and 3). Rows of the array were used to display estimated tilt magnitude per Eq. (23), while columns were used to display tilt directions [Eq. (24)]. Front is 0 deg and right 90 deg. Six prosthesis factor configurations were evaluated in this pilot study: 16 columns (factors placed every 22.5 deg), 8 columns (factors placed at 0, 45, 90, 135, 180, 225, 270, 315 deg), 6 columns (factors placed at 0, 67.5, 112.5, 180, 247.5, 292.5 deg), 4 columns (0, 90, 180, 270 deg), 4 columns interpolation firing scheme (0, 90, 180, 270 deg), and no VTTF. The standard firing scheme operated on a "nearest neighbor" principle. That is, the direction of the subjects' tilt was compared to the particular factor column configuration in use and the best matching column was activated. One alternative firing scheme was used for the four-column factor configuration based on the principle of interpolation; two columns were activated as long as

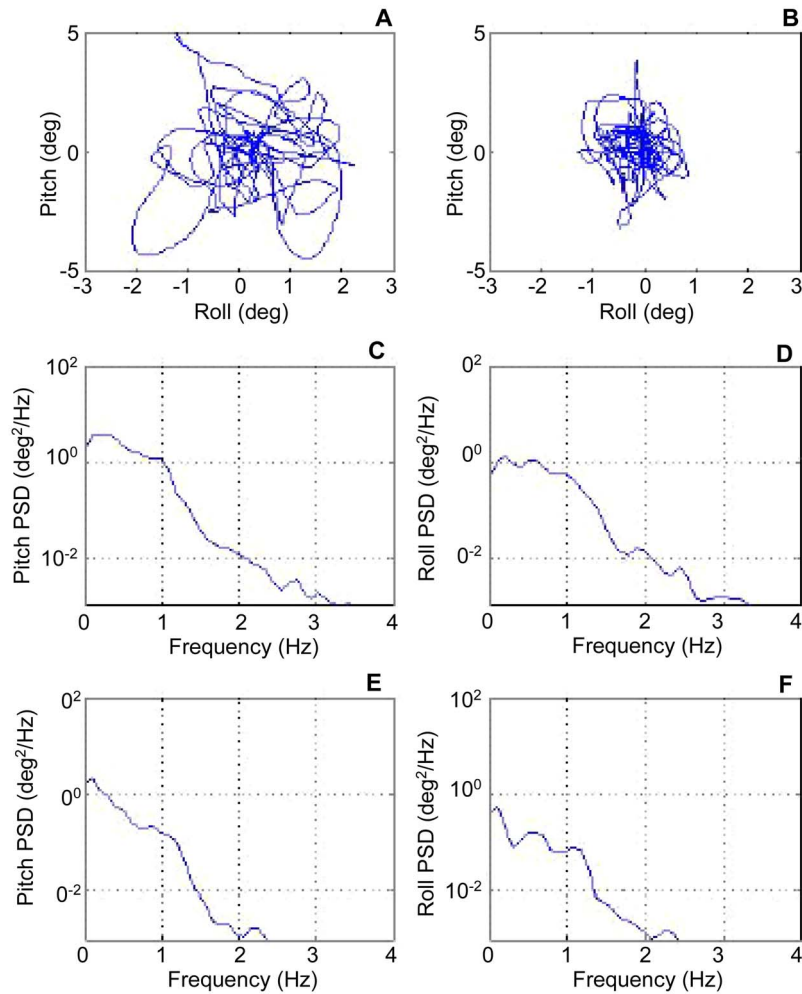


Fig. 12 Pitch and roll angles for a subject having normal balance function (A) without and (B) with VTTF. In both cases, the subject is standing on a platform that is driven by a signal that moves it randomly in the horizontal plane. Spectral analyses (C–F) of the motions shown in A and B, respectively. Panels C and E, respectively, show pitch and roll power without VTTF, while panels D and F show pitch and roll with VTTF display

the tilt direction was not aligned with the coordinate axes.

Prior to testing, the magnitude of the VTTF display was adjusted according to the subject's cone of stability. An elliptical fit to four static leaning values during quiet standing was used to map the lowest, middle, and highest factor row activation thresholds to approximately 1 deg, 3–5 deg (50% of maximum static tilt angle), and 5–7 deg (85% of the maximum static tilt angle), respectively. Next, subjects participated in a 5 to 10 min training session. All factor configurations were practiced during quiet stance in the eyes open and closed configurations. Subjects were instructed to move to null out the vibrations, regardless of the tactor column configuration. Estimates of tilt were used as feedback (proportional feedback).

One subject performed 3 repetitions of each factor configuration according to the following sequence: no tactors (no VTTF), 16 columns, 4 columns, 8 columns, 4 columns interpolation firing scheme, 6 columns, and no tactors. All trials were performed with the subject's eyes closed and arms crossed on the chest. The other subject performed 2 repetitions of each factor configuration in the opposite order: no tactors, 6 columns, 4 columns interpolation firing scheme, 8 columns, 4 columns, 16 columns, and no tactors.

The root-mean-square (rms) of the resultant tilt vector (square root of the squared sum of roll and pitch) was calculated for a standard portion of all trials (24 s of the 30 s trial). The first three

trials, which were performed without VTTF, were averaged and used to normalize the rms of the resultant tilt vector for all subsequent trials.

Approximately 3 months following the pilot study, both subjects returned to participate in an additional study, which controlled for the effect of training (exposure to multiple surface perturbation trials). No prosthesis training occurred prior to this testing session. Each subject donned the prosthesis and completed an identical number of no VTTF trials (20 for one subject, 14 for the other subject) in the eyes-closed configuration using the original surface perturbation stimulus. The trials associated with this study are referred to as control trials.

Test Results. Figure 12, panel A, shows a subject's roll angle versus pitch angle (as estimated by the body-mounted 6-DOF motion sensors) while exposed to random platform surface perturbations without VTTF. In panel B, the VTTF has been turned on and is displayed using eight columns of tactors (spatial resolution of 45 deg). Visual inspection reveals that VTTF reduces the peak roll and pitch. For example, the rms roll and pitch angles are 0.88 and 1.51 deg for the trial without VTTF. These rms values were reduced to 0.39 and 0.98 deg, respectively, with the use of VTTF. The corresponding spectral analyses of these pitch and roll responses are shown in panels C–F. Spectral analysis (MATLAB®, ver-

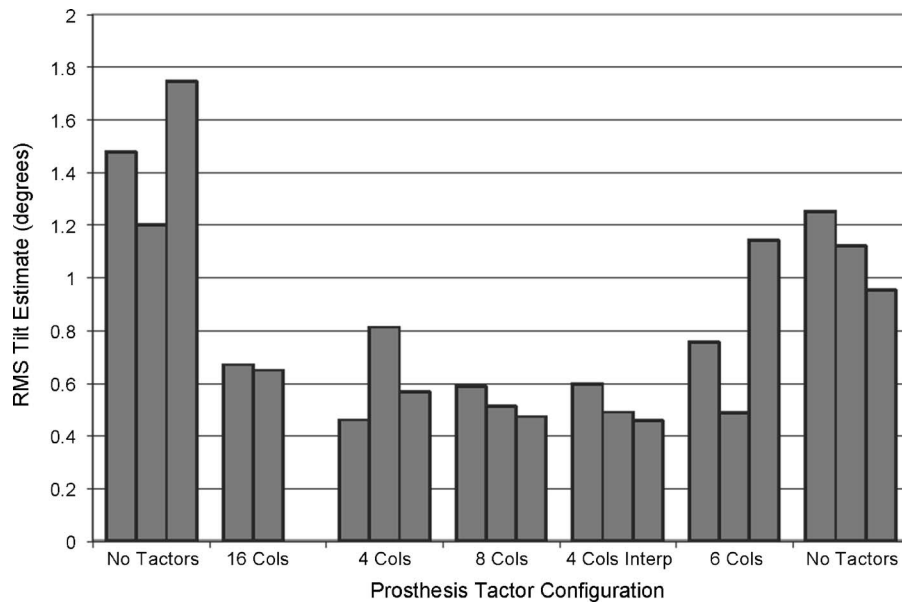


Fig. 13 The rms of the resultant tilt estimate for one subject across all trials

sion 7, function *pwelch* using default parameters, with 100 Hz sampling frequency) was applied to the pitch and roll data. The spectral analysis shows that the greatest decrease in power is observed at the lowest frequencies up through approximately 0.5 Hz. However, some reduction in power is also noticeable up to approximately 2.0 Hz. An analysis of the fine structure of the movement pattern shown in panel B reveals that the subject tends to make reversals in direction when they exceed a threshold of about 1 deg. This threshold corresponds to the “dead zone” of body tilt in which no tactors are firing to provide VTTF.

Figure 13 displays the rms of the resultant tilt estimate for one subject across all trials. The trials are ordered sequentially in time from left to right. It is clear from the figure that the subject’s rms tilt was decreased during the VTTF trials compared with the first and last block of no-tactor (no VTTF) trials. Note that the rms of the resultant tilt estimates corresponding to the last block of no-tactor trials were lower than those corresponding to the first block of no-tactor trials. This could indicate the potential mastery of the perturbation stimulus (learning) and/or postural control improvement due to previous training with the sensory substitution device (adaptation).

The rms resultant tilt estimates from the control study (performed three months later) were fit with a linear regression. The equation of the fit was used to estimate the percentage improvement from the beginning to the end of the control trials. The subject discussed above improved 34.2% (1.71%/trial) from start to end due to exposure to the surface perturbation stimulus alone. The average of this subject’s first three no-tactor trials (Fig. 13) was 1.48 deg. The average of this subject’s VTTF trials (all configurations) was 0.62 deg. One would expect a 14% reduction in sway based on the control study if only exposure to the perturbation stimulus (learning) were responsible for the improvement. Similar results were obtained for the other subject. An additional study is necessary to control for the effect of vibrotactile stimulation, i.e., the effect of meaningful versus nonsensical feedback via vibrotactile stimulation must be evaluated.

Figure 14 shows the average of the two subjects’ normalized rms of the resultant tilt vector for the first block of no-tactor trials, VTTF trials (all configurations), and the last block of no-tactor trials. The results indicate that the prosthesis can help reduce the sway of healthy subjects and that some combination of postural adaptation and learning contribute to the lower rms values associated with the last block of no-tactor trials.

Summary

VTTF appears to reduce the rms of the resultant tilt vector in response to random surface perturbations in the horizontal plane. For subjects with normal vestibular function, the use of VTTF is more effective for reducing the rms of the resultant tilt vector compared with repeated training without VTTF using the same perturbations stimulus. This pilot study, which employed only two healthy subjects, does not permit us to draw any conclusions regarding the spatial resolution required for vestibulopathic subjects to reduce sway in response to multidirectional surface perturbations. Our preliminary results justify further investigations using vestibulopathic subjects.

Conclusions

The wearable vestibular prosthesis has shown promise as both a laboratory testing tool and ultimately as a rehabilitation prosthesis. Thus far, the most dramatic results were obtained in standard clinical tests where balance-impaired subjects were deprived of vision and proprioceptive inputs. In single-axis tests, balance-impaired subjects who fell when not aided were able to stand with the prosthesis.

Multiaxis algorithms for detecting the vertical have been developed, verified by simulation and test station, and applied to healthy subjects. These algorithms greatly reduce tilt errors caused by gyro drift and by undesired lateral accelerations. Vibrotactile feedback reduced the rms tilt response by 58% in response to random horizontal surface perturbations. These positive results justify further investigations using vestibulopathic subjects. Using the prostheses described herein, testing is being performed at MEEI, Boston University, and Portland Health and Sciences University. These tests aim at further understanding the subject-prosthesis interactions in normal and balance-impaired subjects.

Acknowledgment

This investigation was supported by NIH Research Grant No. R01 DC06201-01. NeuroCom International graciously donated their Balance Master software.

Appendix A: Convention For Quaternions

Since there are several definitions of quaternions reported in the literature [52,53], a precise definition of our convention is in-

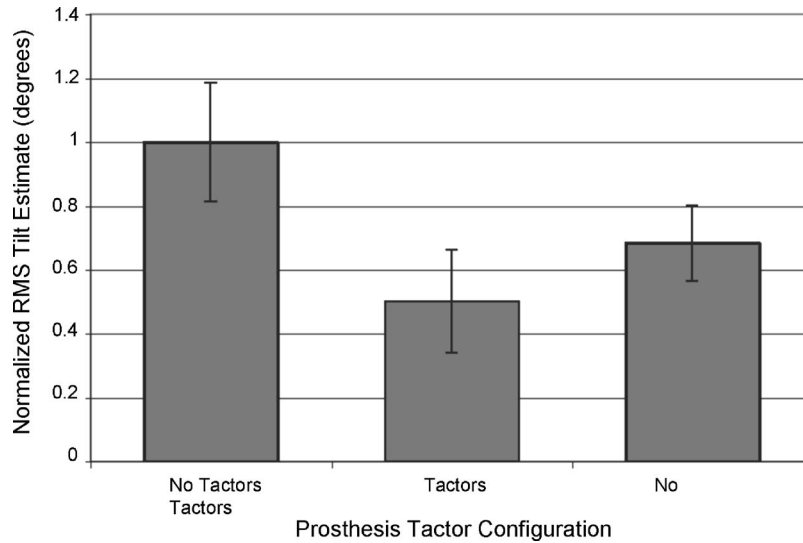


Fig. 14 Average of the two subjects' normalized rms of the resultant tilt vector for the first block of no-factor trials, the VTTF trials, and the last block of no-factor trials. Error bars represent the standard deviation across averaged trials

cluded. A quaternion has four parameters and can be likened to a 4×1 vector. Herein, the first element is considered real, and the last three elements may be considered as complex (i, j, k are sometimes used for the three components). Consider a general quaternions Q defined as:

$$Q = [q_1 \ q_2 \ q_3 \ q_4] \quad (25)$$

A quaternion P is defined similarly. Quaternion multiplication, which is not commutative, is defined as:

$$Q^{**}P = \begin{bmatrix} p_1q_1 - p_2q_2 - p_3q_3 - p_4q_4 \\ p_2q_1 + p_1q_2 + p_4q_3 - p_3q_4 \\ p_3q_1 - p_4q_2 + p_1q_3 + p_2q_4 \\ p_4q_1 + p_3q_2 - p_2q_3 + p_1q_4 \end{bmatrix} \quad (26)$$

The conjugate of the quaternion Q defined in Eq. (25) is given by:

$$\text{conjugate}(Q) = [q_1 \ -q_2 \ -q_3 \ -q_4] \quad (27)$$

For a quaternion used to define rotation:

$$q_1^2 + q_2^2 + q_3^2 + q_4^2 = 1 \quad (28)$$

A vector is represented by $q_1=0$. Parameters 2 through 4 are the vector components in Cartesian coordinates. Often q_1 is defined as the scalar part and the remainder as the vector portion. A vector defined in coordinate frame A is related to that in frame B by:

$$\vec{V}_B = Q^{**} \vec{V}_A \text{conjugate}(Q) \quad (29)$$

The rotation quaternions are related to the angular velocity of the reference frame by:

$$\dot{Q} = \frac{Q^{**} \vec{\omega}^p}{2} \quad (30)$$

where ω^p is the angular rate of frame A with respect to frame B. The angular rate ω^p is defined in frame A. The rotation quaternions Q transform a vector defined in frame A to a vector defined in frame B.

Appendix B: Efficient Form of Complementary Filter

The high- and low-pass complementary filters [Eqs. (4)–(6) and (20)] were combined in state space to reduce the number of integrations.

$$s\mathbf{x} = \begin{bmatrix} 0 & 1 & 0 \\ -\omega_N^2 & -2\zeta\omega_N & 0 \\ \omega_N^3 & \omega_N^2 + 2\zeta\omega_N^2 & -\omega_N \end{bmatrix} \mathbf{x} + \begin{bmatrix} 0 \\ 1 \\ 0 \end{bmatrix} \theta_{a-i} + \begin{bmatrix} \frac{1}{\omega_N^2} \\ 0 \\ 1 \end{bmatrix} \frac{d\theta_{g-i}}{dt} \quad (31)$$

$$\theta_{T-i} = [0 \ 0 \ 1] \mathbf{x}$$

where \mathbf{x} =state vector

i = index indicating for example the quaternion

θ =angle or quaternion

a, g, T =subscripts indicate determined by accelerometers, gyros, or total

Inserting the angular rate into the filter avoids an integration that may lead to numerical overflow.

References

- [1] Wilson, V., Peterson, B., et al., 1979, "Analysis of Vestibulocollic Reflexes by Sinusoidal Polarization of Vestibular Afferent Fibers," *J. Neurophysiol.*, **42**, pp. 331–46.
- [2] Hoffman, H. J., Ko, C. W., MacTurk, R. H., Sklare, D. A., Chiu, M. S., and Cosgrove, C. M., 2000, "Aging and Chronic Problems With Balance and Dizziness Based on the 1994/1995 Disability Supplement," *Am. J. Epidemiol.* in 33rd Annual Meeting, June 15–17, Seattle, WA.
- [3] NCHS, 1994/1995, "National Health Interview Survey, Disability Supplement," accessed, www.cdc.gov/nchs/nhis.htm.
- [4] Yardley, L., Burgneay, J., et al., 1998, "Feasibility and Effectiveness of Providing Vestibular Rehabilitation for Dizzy Patients in the Community," *Clin. Otolaryngol.*, **23**, pp. 442–448.
- [5] Wall, C., Merfeld, D. M., et al., 2002, "Vestibular Prostheses: The Engineering and Biomedical Issues," *J. Vestib. Res.*, **12**, pp. 95–113.
- [6] Bach-y-Rita, P., 2003, "Late Post-Acute Neurologic Rehabilitation: Neuroscience, Engineering and Clinical Programs," *Arch. Phys. Med. Rehabil.*, **84**, pp. 1100–1108.
- [7] Bach-y-Rita, P., Kaczmarek, K. A., et al., 1998, "Form Perception With a 49-Point Electrotactile Stimulus Array on the Tongue: A Technical Note," *J. Rehabil. Res. Dev.*, **35**, pp. 427–430.
- [8] Allum, J., 1999, "Method and Apparatus For Angular Position and Velocity Based Determination of Body Sway For the Diagnosis and Rehabilitation of Balance and Gait Disorders," US 5,919,149, July 6.
- [9] Wall, C., III, Weinberg, M. S., et al., 2001, "Balance Prosthesis Based on Micromechanical Sensors Using Vibrotactile Feedback of Tilt," *IEEE Trans. Biomed. Eng.*, **48**, pp. 1153–1161.
- [10] Rupert, A., Guedry, F., and Reschke, M., 1993, "The Use of a Tactile Interface to Convey Position and Motion Perceptions," *North Atlantic Treaty Organization. Advisory Group for Aeronautics Research and Development. Aerospace Medical Panel. Virtual Interfaces: Research and Applications*, Lisbon, Portugal.

- [11] Rupert, A. H., 1996, "Tactile Interface to Improve Situation Awareness," *Aerospace Medical Association*, Washington, DC.
- [12] Kourepenis, A., Borenstein, J., et al., 1998, "Performance of MEMS Inertial Sensors," *AIAA GN&C Conference*, August.
- [13] Karnick, D., Balas, G., et al., 2005, "Honeywell Gun-Hard Inertial Measurement Unit (IMU) Development," accessed February 15, 2005, <http://content.honeywell.com/dses/assets/datasheets/GunHardIMUpaper2.pdf>.
- [14] "MEMS Inertial Products Performance and Production Readiness," accessed February 15, 2005, <http://content.honeywell.com/dses/assets/datasheets/mems-presentation.pdf>.
- [15] Hanse, J. G., 2005, "Honeywell MEMS Inertial Technology & Product Status," accessed February 15, 2005, http://content.honeywell.com/dses/assets/datasheets/mems_technology_product_status.pdf.
- [16] Cholewiak, R. W., and Collins, A. A., 1991, *Sensory and Physiological Bases of Touch*, in *The Psychology of Touch*, edited by M. A. Heller and W. Schiff, Laurence Erlbaum Assn, Hillsdale, NJ, pp. 23–60.
- [17] Kaczmarek, K. A., Webster, J. G., et al., 1991, "Electrotactile and Vibrotactile Displays For Sensory Substitution Systems," *IEEE Trans. Biomed. Eng.*, **38**, pp. 1–16.
- [18] Luinge, H. J., Veltink, P. H., and Baten, C. T., 1999, "Estimating Orientation With Gyroscopes and Accelerometers," *Technol. Health Care*, **7**, pp. 455–459.
- [19] Lobo, J., and Dias, J., 2004, "Inertial Sense Ego-Motion for 3D Vision," *J. Rob. Syst.*, **21**, pp. 3–12.
- [20] Lobo, J., and Dias, J., 2003, "Vision and Inertial Sensor Cooperation Using Gravity as a Vertical Reference," *IEEE Trans. Pattern Anal. Mach. Intell.*, **25**, pp. 1597–1608.
- [21] Vieville, T., Clergue, E., and Facao, P. E. D. S., 1993, "Computation of Ego-Motion and Structure From Visual and Inertial Sensors Using the Vertical Cue," *Proc. International Conf Computer Vision*, pp. 591–598.
- [22] Bachmann, E. R., Duman, I., et al., 1999, "Orientation Tracking For Humans and Robots Using Inertial Sensors," *1999 International Symposium on Computational Intelligence in Robotics and Automation*, 1999.
- [23] Bachmann, E. R., Yun, X., et al., 2003, "Design and Implementation of MARG Sensors For 3-DOF Orientation Measurement of Rigid Bodies," *IEEE International Conf. on Robotics and Automation*, Taipei, Taiwan, 14–19 September.
- [24] Bar-Itzhack, I. Y., and Reiner, J., 1984, "Recursive Attitude Determination From Vector Observations: Direction Cosine Matrix Identification," *J. Guid. Control*, **7**, pp. 51–56.
- [25] Bar-Itzhack, I. Y., and Oshman, Y., 1985, "Attitude Determination From Vector Observations: Quaternion Estimation," *IEEE Trans. Aerosp. Electron. Syst.*, Vol. **AES-21**, pp. 128–135.
- [26] Farrell, J. L., and Stuepnagel, J. C., 1966, "Problem 65-1. A Least Squares Estimate of Satellite Attitude," *SIAM Rev.*, **8**, pp. 384–386.
- [27] Gebre-Egziabher, D., Elkaim, G. H., et al., 2000, "A Gyro-Free Quaternion Based Attitude Determination System Suitable for Implementation Using Low Cost Sensors," *IEEE PLANS 2000*, San Diego, CA, 13–16 March.
- [28] Gebre-Egziabher, D., Hayward, R. C., and Powell, J. D., 2004, "Design of Multi-Sensor Attitude Determination Systems," *IEEE Trans. Aerosp. Electron. Syst.*, **40**, pp. 627–649.
- [29] Marins, J. L., Yun, X., et al., 2001, "An Extended Kalman Filter For Quaternion-Based Orientation Estimation Using MARG Sensors," *IEEE International Conference on Intelligent Robots and Systems*, Maui, Hawaii, 29 Oct.–3 Nov.
- [30] Wahba, G., 1965, "Problem 65-1. A Least Squares Estimate of Satellite Attitude," *SIAM Rev.*, **7**, p. 409.
- [31] Kemp, B., Janssen, A. J., and Kamp, B. v. d., 1998, "Body Position Can Be Monitored in 3D Using Miniature Accelerometers and Earth-Magnetic Field Sensors," *Electroencephalogr. Clin. Neurophysiol.*, **109**, pp. 484–488.
- [32] Williamson, R., and Andrews, B. J., 2001, "Detecting Absolute Human Knee Angle and Angular Velocity Using Accelerometers and Rate Gyroscopes," *Med. Biol. Eng. Comput.*, **39**, pp. 294–302.
- [33] Zijlstra, W., and Bisseling, R., 2004, "Estimation of Hip Abduction Moment Based on Body Fixed Sensors," *Clin. Biomech. (Bristol, Avon)*, **19**, pp. 819–827.
- [34] Markey, W., and Hovorka, J., 1961, *The Mechanics of Inertial Position and Heading Indication*, Methuen, London.
- [35] Britting, K. R., 1971, *Inertial Navigation Systems Analysis*, Wiley-Interscience, New York.
- [36] Vieville, T., and Faugeras, O., 1989, *Cooperation of the Inertial and Visual Systems*, in *Traditional and Non-Traditional Robot Sensors*, edited by T. Henderson, Springer-Verlag, Berlin, pp. 339–350.
- [37] Vieville, T., and Faugeras, O., 1989, "Computation of Inertial Information on a Robot," *5th International Conf. on Robotics Research*, MIT Press, Tokyo.
- [38] Kaddake, P. P., Benda, B. J., et al., 2003, "Vibrotactile Display Coding For a Balance Prosthesis," *IEEE Trans. Neural Syst. Rehabil. Eng.*, **4**, pp. 392–399.
- [39] Weinberg, M. S., and Wall, C., 2002, "MEMS Inertial Sensor Assembly for Vestibular Prosthesis," *The Institute of Navigation 59th Annual Meeting*, Albuquerque, NM, 23–25 June.
- [40] Weinberg, M., and Wall, C., 2003, "Sensor Assembly for Postural Control Balance Prosthesis," *Transducers '03*, Boston, MA, 9–12 June.
- [41] Vivas, J., 2001, "A Precursor to a Balance Prosthesis via Vibrotactile Display," Masters Thesis, Mass. Institute of Technology, May.
- [42] Merfeld, D., Rauch, S., et al., 2003, "Vestibular Prosthesis Based on Micro-mechanical Sensors," *US 6,546,291*, April 8, 2003.
- [43] Kentala, E., Vivas, J., and Wall, C., 2003, "Reduction of Postural Sway By Use of a Vibrotactile Balance Prosthesis Prototype in Subjects with Vestibular Deficits," *Ann. Otol. Rhinol. Laryngol.*, **112**(5), pp. 404–409.
- [44] Wall, C., and Weinberg, M. S., 2003, "Balance Prosthesis for Postural Control," *IEEE Eng. Med. Biol. Mag.*, **22**, pp. 84–90.
- [45] Carnahan, B., Luther, H. A., and Wilkes, J. O., 1969, *Applied Numerical Methods*, Wiley, New York.
- [46] Black, F. O., Wall, C., and Nashner, L. M., 1983, "Effects of Visual and Support Surface Orientation References Upon Postural Control In Vestibular Deficient Subjects," *Acta Oto-Laryngol.*, **95**, pp. 199–201.
- [47] Kuo, A. D., 1998, "Effect of Altered Sensory Conditions on Multivariate Descriptors of Human Postural Sway," *Exp. Brain Res.*, **122**, pp. 185–195.
- [48] Nashner, L. M., Black, F. O., and Wall, C., III, 1982, "Adaptation to Altered Support and Visual Conditions During Stance: Patients With Vestibular Deficit," *J. Non-Cryst. Solids*, **2**, pp. 536–544.
- [49] "Management of Balance and Mobility Disorders Bibliography," Neurocom International, http://www.onbalance.com/clinical_info/library/BibliographyList.aspx
- [50] Wall, C. III, and Kentala, E., 2002, "Control of Sway in Vestibulopathic Subjects Using Vibrotactile Display of Body Tilt," *MidWinter Meeting of the Association for Research in Otolaryngology*, St. Petersburg Beach, FL, 27–31 January.
- [51] Oddsson, L. I. E., Wall, C., et al., 2004, "Recovery From Perturbations During Paced Walking," *Gait and Posture*, **19**, pp. 24–34.
- [52] Battin, R. H., 1999, *An Introduction to the Mathematics and Methods of Astrodynamics*, revised edition, AIAA, Reston, VA.
- [53] Corben, H. C., and Stehle, P., 1960, *Classical Mechanics*, 2nd ed., Dover, New York.